Journal of Soil Sciences and Agricultural Engineering

Machine Learning and Pan-Sharpening of Sentinel-2 Data for Land Use Mapping in Arid Regions: A Case Study in Fayoum, Egypt

Mahmoud, A. G.*

Soils and Water Department, Faculty of Agriculture, Fayoum University, Postal Code: 63514, Fayoum, Egypt.

Cross Mark

ABSTRACT

Land use/cover mapping is essential in monitoring land resources and consequently for their proper management strategies. Remotely sensed data play a significant role in mapping land use/cover, however, some constraints of selecting the data are the cost and resolution in addition to the software availability. The study area, located in Fayoum Governorate, Egypt, is characterized by fragmented and small parcels, in addition to the rapid changes in land use particularly during the current decade. Recently, the new sentinel-2 mission provides high-resolution optical imagery with spatial resolutions of 10m, 20m and 60m over 13 spectral bands. Therefore, using such fine resolution bands in land cover classification gives an advantage to deal with the small parcels problem. The current study aims at exploring the freely available Sentinel-2 data for land use/cover mapping with the aid of QGIS software (as an open-source). In this regard, different data fusion techniques; Bayesian fusion (Bayes), the Local Mean and Variance Matching (LMVM), and the ratio component substitution (RCS) were evaluated followed by image classification using different classifiers; Support Vector Machine (SVM), Artificial Neural networks (ANN), Decision Tree (DT), and Random Forest (RF). The results showed that the Bayes and LMVM produced higher spectral and spatial resolutions in comparison to the original data, respectively. In addition, the results revealed high classification accuracy, as the SVM produced highest accuracy of 96.8% using LMVM-sharpened data. Further investigation is recommended to utilize multi-temporal Sentinel-2 data in land use/cover mapping and agricultural monitoring.

Keywords: Sentinel-2; QGIS; land use/cover; fusion; Fayoum; Egypt.

INTRODUCTION

Land use/cover (LU/LC) mapping is interested in the biophysical cover of the Earth's terrestrial surface, including vegetation, inland water, bare soil, and human infrastructure (Gómez *et al*., 2016, Steinhausen *et al*., 2018). In addition, it is essential in monitoring land resources and consequently for developing their proper management strategies (Noi and Kappas, 2018, Steinhausen *et al*., 2018, Das and Angadi, 2021). From various points of view, studying land cover is a crucial issue, i.e., LC interaction with the atmosphere, with a regulation role of the hydrologic cycle and energy budget. Also, it has a main role in the carbon cycle acting as both sources and sinks of carbon. In addition, it is an indicator for some resources such as food availability, timber, and fuel (Sudhakar and Kameshwara, 2010). In agriculture domain, LU/LC is a vital input for defining the crop water requirements and irrigation water management (Demarez *et al*., 2019, Moumni and Lahrouni, 2021). Many studies reported that changes in LU/LC affect some soil physical and chemical properties (Worku *et al*., 2014). Moreover, Vacca *et al.* (2014) used land cover map as relevant data to soil formation factors in order to generate a soil map.

Remotely Sensed (RS) data play a significant role in achieving LU/LC mapping (Sudhakar and Kameshwara, 2010, Steinhausen *et al*., 2018), where different RS data types (i.e., optical and microwave data) have been utilized (Chatziantoniou *et al*., 2017, Chen *et al*., 2017, Noi and Kappas, 2018). Selection of the proper RS data for a particular application is controlled by some factors such as the cost and resolutions (Rogan and Chen, 2004, Delincé, 2017, Pan *et al*., 2021). The recent progress in RS technologies improves the RS data characteristics, i.e., spatial, spectral, and temporal resolution, in addition to the free availability of some optical and microwave data (Forkuor *et al*., 2018, Chrysafis *et al*., 2019). Many remotely sensed data that acquired by sensors such as Landsat, GeoEye, and SPOT have the so-called "Panchromatic band", which has higher spatial resolution than that in the multispectral bands of the same sensor. However, in case of some sensors i.e., Sentinel-2, and Rapid-Eye, the image is acquired only in multispectral mode (Duran *et al*., 2017, Gasparovic and Jogun, 2018). Therefore, various fusion (pan-sharpening) methods have been developed in order to enhance the multispectral bands by combining them with panchromatic ones (Gasparovic and Jogun, 2018, Wan *et al*., 2021), which consequently improves the human visualization (Mercovich, 2015, Orynbaikyzy *et al*., 2020) in addition to improving the classification accuracy (Gasparovic and Jogun, 2018, Dibs *et al*., 2021). The fusion method is better as much as it could preserve the spectral characteristics and the spatial information of the multispectral and the panchromatic data, respectively (Nikolakopoulos and Oikonomidis, 2017, Wu *et al*., 2021, Nguyen *et al*., 2021).

In arid and heterogeneous landscapes, it is a challenge to obtain a proper classification accuracy from remotely sensed data classification. Where fragmented land parcels, variation in spatial patterns, and variable vegetation cover are the main problems (Thakkar *et al*., 2017, Gumma *et al*., 2020). Several image classification techniques have been developed; thus, selection of appropriate classifier is important to improve the obtained accuracy. Recently, non-parametric techniques i.e., support vector machine, decision tree, and neural network, have

received a great attention and progressively become vital methods for classifying multisource data (Lu and Weng, 2007, Noi and Kappas, 2018, Moumni and Lahrouni, 2021, Mazarire *et al*., 2020). During the last 10 years, development and availability of open-source software has increased (Duarte and Teodoro, 2021), and provide different techniques for image processing and classification. Moreover, the integration capabilities maximize the overall benefits from these software packages (Rapinel and Hubert-Moy, 2021).

The study area, located in Fayoum Governorate, Egypt, is characterized by fragmented farms or smallholders, in addition to the rapid changes in land use particularly during the last ten years. The new sentinel-2 mission provides high-resolution optical imagery with resolutions of 10 m (four bands), 20 m (six bands) and 60 m (three bands). Therefore, using the fine resolution bands for land cover classification gives an advantage to work with such small parcels problem (Steinhausen *et al*., 2018). In addition, Detailed spectral

information provides opportunities for improving accuracy when discriminating between different crop types (Karakus and Karabork, 2016). The current study aims at investigating the freely available Sentinel-2 data for land use/cover mapping with the aid of QGIS software (open-source), where various pan-sharpening and classification approaches were considered and evaluated.

MATERIALS AND METHODS

1-Location of the study area

The study area is located in Fayoum Governorate, Egypt (Figure 1), between the latitudes 29.26° N and 29.39° N, and the longitudes 30.74° E and 30.89° E with an area of about 19600 ha. This area was selected to represent different land cover types with various parcels' size. The main land cover types are crops (agricultural fields), orchards, bare soil (this class includes both the area under preparation for cultivation, and the area with spares vegetation), urban, roads and water bodies.
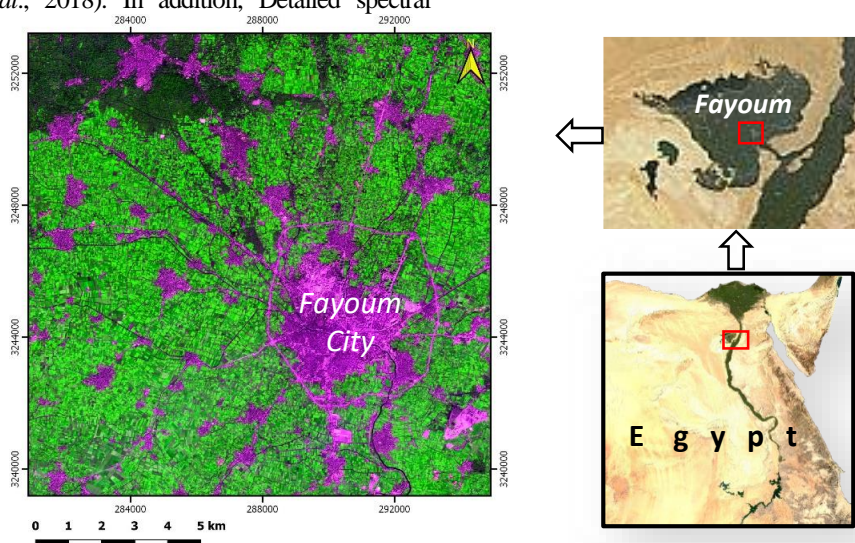

Figure 1. Location of the study area

2-Remotely sensed data

Sentinel-2A level-1C images used in the current study were acquired on February 3rd and August 12th, 2017, with spatial resolutions of 10 m (Bands: 2, 3, 4 and 8), 20 m (Bands: 5, 6, 7, 8a, 11 and 12) and 60 m (Bands: 1, 9 and 10). These data were downloaded from the website of the U.S. Geological Survey (USGS) (http://glovis.usgs.gov/). These two acquisition dates were selected to represent two agricultural growing seasons, namely winter and summer.

3-Image processing

Atmospheric correction was applied using the widely used Dark Object Subtraction (DOS) method, which is available in the Semi-Automatic Classification Plugin (SCP) in QGIS platform, where the digital number (DN) was converted to reflectance (Congedo, 2020, Valdivieso-Ros *et al*., 2021). Then, the two images were clipped to the study area. Different pan-sharpening methods namely Bayesian, Local Mean and Variance Matching (LMVM), and Ratio Component Substitution (RCS) method were applied to enhance the resolution of the 20 m bands using the 10 m bands. Figure (2) illustrates the proposed methodology. Additionally, the graphical modeler in QGIS was utilized to build a model which applies the pan-sharpening method and then merge the output with the original 10 m bands in order to get a new layer stack

having 10 bands with spatial resolution of 10 m. This model was run as a batch process to be applied for all fusion methods.
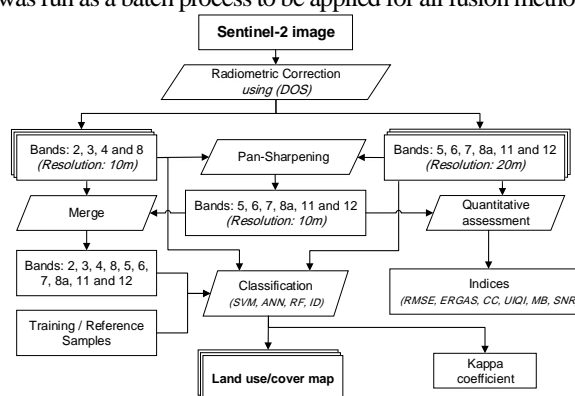

Figure 2. Flowchart of the proposed methodology

4-Evaluation of sharpened images

In order to evaluate different methods of data fusion, the obtained fused images were compared to both the original 10 m and 20 m bands. According to Nikolakopoulos and Oikonomidis (2017), evaluation of the fusion quality starts with visual assessment, which depends on some parameters such as changes in color tonality, presence of local or global color distortion, linear distortion in i.e., roads and buildings, in addition to the over-all appearance of the image. Therefore, visual evaluation was

applied for the false color composites of the fused images against the original 20 m bands. Moreover, six indices were calculated for quantitative analysis of the fused images as follows:

RMSE: Root mean square error -as a good indicator of spectral quality- is used to compare the reference and fused images (Equation 1) where the variation in pixel values is computed. The lower RMSE value the closer fused image to the reference image.

$$RMSE = \sqrt{\frac{1}{MN}\sum_{i=1}^{M}\sum_{j=1}^{N}(I_r(i,j)-I_f(i,j))^2} \quad \textbf{Eq. 1}$$

Where *M, N*: the number of lines and columns of image, respectively, and *I$_r$, I$_f$*: the reference and fused images, respectively (Jagalingam and Hegde, 2015).

ERGAS: Erreur Relative Globale Adimensionnelle de Synthèse, English: relative dimensionless global error of synthesis (Pohl and John, 2017), is one of the widely used methods to assess the quality of pan-sharpened images (Equation 2). Where the lower value of ERGAS indicates fewer distortion in the spectral data of the fused image (Ni-Bin and Kaixu, 2018).

$$ERGAS = 100\frac{h}{l}\sqrt{\frac{1}{N}\sum_{k=1}^{N}\left(\frac{RMSE}{\mu(K)}\right)^2} \quad \textbf{Eq. 2}$$

Where *h* and *l*: the spatial resolutions of the fine and coarse images, respectively. *N*: total number of bands in the coarse image, *μ(k)*: the spectral mean of the kth original band of the coarse image, and RMSE: root-mean-square error between the kth band of the original coarse image and the fused image.

MB: Mean Bias calculates the difference between the mean of the reference and fused images (Equation 3). The value of zero indicates that fused and reference images are similar. Mean value refers to the grey level of pixels in reference and fused images (Jagalingam and Hegde, 2015).

$$MB = \frac{I_{r_{mean}} - I_{r_{mean}}}{I_{r_{mean}}} \quad \textbf{Eq. 3}$$

CC: Correlation Coefficient computes the spectral similarity between the reference and fused images (Equation 4). The value close to +1 indicates that reference and fused images are the same, while values less than 1 represent increases in variation (Jagalingam and Hegde, 2015).

$$CC(I_r\ I_f) = \frac{\sum_{i=1}^{M}\sum_{j=1}^{N}(I_{r(i,j)}-\bar{I}_r)(I_{f(i,j)}-\bar{I}_f)}{\sqrt{\left[\sum_{i=1}^{M}\sum_{j=1}^{N}(I_{r(i,j)}-\bar{I}_r)^2\right]\left[\sum_{m=1}^{M}\sum_{n=1}^{N}(I_{f(i,j)}-\bar{I}_f)^2\right]}} \quad \textbf{Eq. 4}$$

SNR: Signal to noise ratio measures the ratio between information and noise of the fused image (Equation 5). Similarity between reference and fused image increases as the SNR value increases.

$$SNR = 10\ log_{10}\left(\frac{\sum_{i=1}^{M}\sum_{j=1}^{N}(I_r(i,j))^2}{\sum_{i=1}^{M}\sum_{j=1}^{N}(I_r(i,j)-I_f(i,j))^2}\right) \quad \textbf{Eq. 5}$$

UIQI: Universal image quality index is used to calculate the amount of transformation of relevant data from reference image into fused image (Equation 6). The values range from -1 to 1, where the reference and fused images are similar if UIQI value is 1 (Jagalingam and Hegde, 2015).

$$UIQI = \frac{4\ \sigma_{I_r I_f} * \mu_{I_r} * \mu_{I_f}}{\left(\sigma_{I_r}^2 * \sigma_{I_f}^2\right)\left[\left(\mu_{I_r}\right)^2 + \left(\mu_{I_f}\right)^2\right]} \quad \textbf{Eq. 6}$$

In order to calculate these indices for all fused images, a python script was written in QGIS to calculate these indices for each image, then the script was run for all images with the capability of batch processing. The script also enables to save all the results in a text file with a header line for each index then each line has the corresponding index value in addition to the name of the analyzed image.

5-Image classification

The classification process was applied for the different data sets with different band combinations (original 10 m bands only, original 20 m bands, and stack of both original 10 m bands and pan-sharpened data with different methods) using different supervised classification methods. Meanwhile, different regions of interest (ROI) were selected representing both training and reference data for classification and accuracy assessment, respectively. The ROI layer which utilized for the first image was utilized for the second image after applying the required update, which was mainly in crops and bare soil classes according to the growing season. A total number of 498 and 557 polygons (with 1960 and 1980 pixels) were collected from first and second image, respectively. The total number of pixels represented by the ROIs were utilized as 70% for training and 30% as validation data.

The applied classifiers are support vector machine (SVM), artificial neural network (ANN), random forest (RF), and decision tree (DT). The classification was applied in QGIS using the supported classification capabilities by Orfeo toolbox. The classification and accuracy assessment were modeled in QGIS, where a graphical model was built to apply the four classifiers, then it was exported as a python script. This script was modified and extended to calculate and save (as a text file) the overall accuracy for each classifier in addition to the name of the corresponding classified image. Where the accuracy assessment was calculated from the confusion matrix obtained by the Orfeo toolbox. Finally, the model was run in a batch model for all images.

RESULTS AND DISCUSSION

Sentinel-2 images were pan-sharpened using different techniques; moreover, different classifiers were applied and evaluated for land use/cover mapping.

1-Evaluation of pan-sharpening methods

Visual evaluation was applied to compare the fused images with the original 10 m and 20 m bands for spatial and spectral characteristics, respectively. Comparing with higher resolution bands, the pan-sharpening methods improved the resolution of 20 m bands with various qualities as shown in Figure (3).
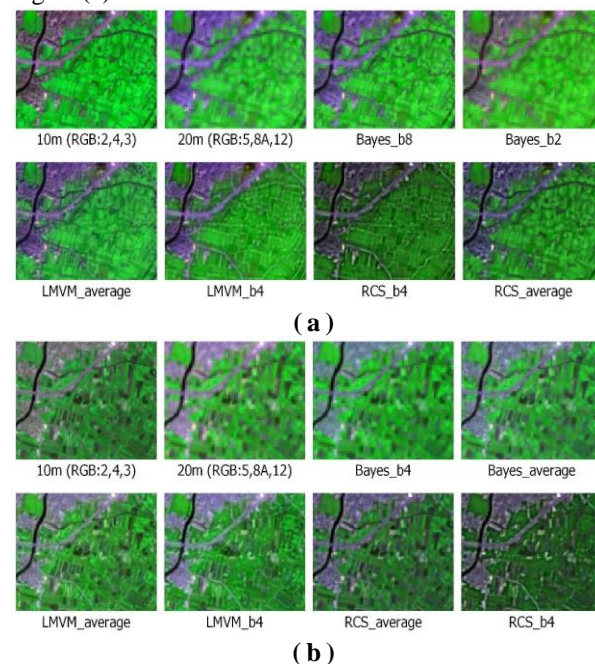

Figure 3. Pan-sharpening results, (a) first acquisition (February 3rd, 2017), (b) second acquisition (August 12th, 2017)

In the two acquisition dates, it is observable that the LMVM method using average-image (as panchromatic band) enhanced the spatial resolution and emphasized the edges; where, i.e., irrigation canals, roads, urban, and parcels boundaries are recognized better. Similar findings were reported by Witharana *et al.* (2014) where the visual evaluation of pan-sharpened GeoEye-1 imagery revealed that the LMVM fusion algorithms showed the best quality. On the other hand, the spectral evaluation revealed that the quality of pan-sharpened images varies from one method to another, i.e., the "Bayes_b8" image expressed spectral details close to the original 20 m bands more than the other methods.

In the quantitative analysis, the pan-sharpened images were compared with the original low-resolution bands (20 m bands) to evaluate how much the pan-sharpening method maintained the spectral information close to the original data. The calculated indices (Tables 1 and 2) showed variation between different fusion methods, in addition to the variation within each method according to the used high-resolution band in sharpening process.

Table 1. Quantitative evaluation indices for pan-sharpening methods (image: 03.02.2017)

Pan-sharpening method	Panchromatic band	Quantitative evaluation indices					
		RMSE	ERGA	CC	UIQI	MB	SNR
Bayes	2	0.052	4.668	0.795	0.794	0.0000	18.260
	3	0.048	4.482	0.798	0.797	0.0000	19.530
	4	0.032	3.626	0.809	0.809	0.0000	19.829
	8	0.022	3.029	0.813	0.813	0.0000	23.257
	Average	0.030	3.512	0.803	0.802	0.0000	19.042
	Summation	0.030	3.512	0.803	0.802	0.0000	19.042
LMVM	2	0.100	6.470	0.720	0.719	0.0019	15.190
	3	0.079	5.741	0.748	0.747	0.0007	15.975
	4	0.101	6.498	0.717	0.716	0.0019	15.289
	8	0.074	5.558	0.766	0.765	0.0013	16.334
	Average	0.060	5.002	0.777	0.777	0.0008	16.655
	Summation	0.060	5.002	0.777	0.777	0.0008	16.655
RCS	2	0.124	7.196	0.745	0.730	-0.0005	13.829
	3	0.113	6.849	0.759	0.743	-0.0032	14.248
	4	0.276	10.714	0.655	0.624	0.0050	10.826
	8	0.129	7.325	0.749	0.728	-0.0025	13.569
	Average	0.080	5.786	0.780	0.766	-0.0050	15.401
	Summation	0.080	5.786	0.780	0.766	-0.0050	15.401

Table 2. Quantitative evaluation indices for pan-sharpening methods (image: 12.08.2017)

Pan-sharpening method	Panchromatic band	Quantitative evaluation indices					
		RMSE	ERGA	CC	UIQI	MB	SNR
Bayes	2	0.016	2.602	0.815	0.815	0.0000	25.703
	3	0.015	2.478	0.817	0.817	0.0000	35.045
	4	0.011	2.178	0.820	0.820	0.0000	26.451
	8	0.015	2.468	0.798	0.797	0.0000	25.473
	Average	0.017	2.652	0.813	0.812	0.0000	24.382
	Summation	0.017	2.652	0.813	0.812	0.0000	24.382
LMVM	2	0.072	5.486	0.626	0.623	0.0014	16.194
	3	0.062	5.097	0.660	0.658	0.0016	16.691
	4	0.072	5.491	0.621	0.617	0.0013	16.313
	8	0.039	4.043	0.772	0.772	0.0000	18.801
	Average	0.033	3.720	0.761	0.761	0.0004	18.537
	Summation	0.033	3.720	0.761	0.761	0.0004	18.537
RCS	2	0.117	6.978	0.647	0.631	0.0033	13.774
	3	0.068	5.339	0.722	0.712	0.0003	15.740
	4	0.200	9.120	0.550	0.522	0.0079	11.821
	8	0.069	5.364	0.762	0.727	-0.0029	15.663
	Average	0.038	3.995	0.782	0.768	-0.0028	17.855
	Summation	0.038	3.995	0.782	0.768	-0.0028	17.855

For both acquisition dates, the Bayesian method performed better than LMVM and RCS methods, which means that Bayes method preserved the spectral data as much close as the original 20 m bands. Also, it is noticeable that the indices of fused images using both average and summation of the four 10 m bands are the same, which indicates that in further work one of them might be enough to be used for pan-sharpening and quantitative analysis. In general, using the average for pan-sharpening produced high quality sharpened image with LMVM and RCS methods, while with Bayesian method bands 4 and 8 performed better.

2-Land use/cover classification

The classification process was applied for each of the following datasets: the original 10 m bands, the 20 m bands, in addition to the images (having 10 bands) obtained from stacking both 10 m bands and each pan-sharpened image with different methods. Images were classified without applying filtering to keep the original data and test the variation resulted from pan-sharpening methods. However, filtering techniques might increase the classification accuracy.

Figure (4) shows the variation in overall accuracy obtained by different classifiers and different fusion techniques. For the first acquisition date (February 3rd), the accuracy values in case of original 20 m bands were higher than that of 10 m bands, which might be attributed to the spectral ranges of the 20 m bands (NIR, and SWIR). However, in the image of August 12th there was no such trend. Furthermore, the combined images (original 10 m bands and pan-sharpened bands) produced higher accuracy as more spectral regions were included namely VIS, NIR, and SWIR, in addition to their enhanced spatial resolution. On the other hand, performance of different classification techniques showed significant variation. As illustrated in Figure (4), almost SVM classifier produced higher accuracies among all classifiers, particularly, in the second acquisition date where the differences are significantly appearing. Additionally, it is noticeable that the LMVM pan-sharpened images performed better with all classifiers in the two imaging dates, however, the Bayesian method was better in quantitative sharpening quality.

The results demonstrated that the Sentinel-2 data with high spatial resolution revealed good classification results for the small-parcels areas using image of one single acquisition date. The SVM classification of LMVM pan-sharpened images using band 8 resulted in six classes (Figure 5) as they were defined by the training data with overall accuracy of 96.8% and 95.7% for first and second acquisition dates, respectively. In general, the agricultural area in the first acquisition data (February) was 13211 ha (including orchard area of 1763 ha, and field crops as 11448 ha). While in the second image, the agricultural area represented 12699 ha (including orchard area of 1306 ha, and field crops as 11393 ha). The difference in orchard areas could be attributed to the variation in the phenological stage of the fruit trees. The first acquisition represents the end of winter period with low soil and plant management, and the orchard areas are more recognizable from field crops. While the second acquisition (August 12th) followed the spring vegetative growth period and the trees have received the required management and fertilizations which enhance the new vegetative growth that makes some interference with the growing crop in the classification process. Therefore, the extraction of orchard

area can be improved through using temporal Sentinel-2 data, moreover, Sentinel-1 could provide a valuable data for studying the orchards based on the volumetric scattering behavior of the microwaves. On the other hand, the fallow land areas are 2617 ha and 3195 ha in the first and second image, respectively. The higher area in summer could be referred to as some areas represent post-harvest areas of some crops (i.e., Maize) and other areas are under preparation for the next cropping season.

The irrigation canals were identified well in some areas which can be considered as an advantage of using S2 data, however some canals could not be classified in relation to the canal's width. The urban areas were estimated in both images with an area of 2821 ha and 2867 ha in the first and second acquisition dates, respectively. It is noticeable that, in some places there is miss-classification between urban areas and roads, which might be attributed to the nature of both classes and the reflectance contribution of the roads in urban areas as mixed pixels.
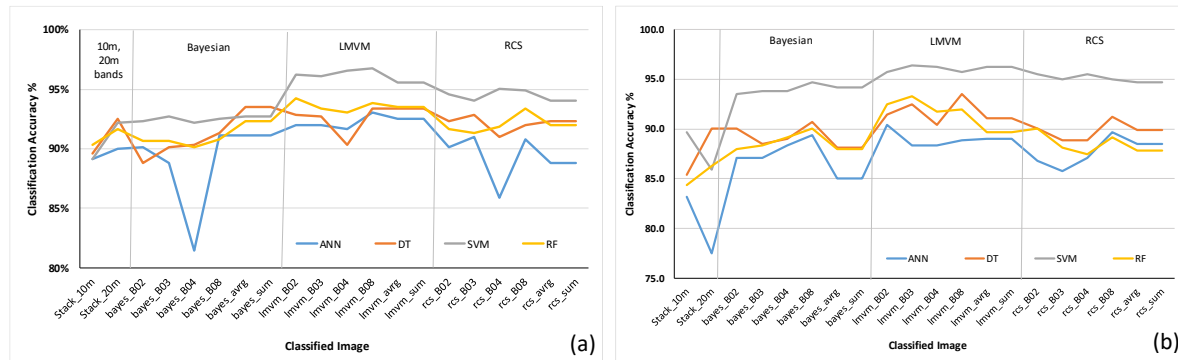

Figure 4. Classification accuracy for different classifiers and fusion techniques, data acquired on (a) 03.02.2017 and (b) 12.08.2017. The name of classified image is referred to as abbreviations, i.e., "bayes_B02" indicates the Bayesian fusion method using B02 as the high-resolution band
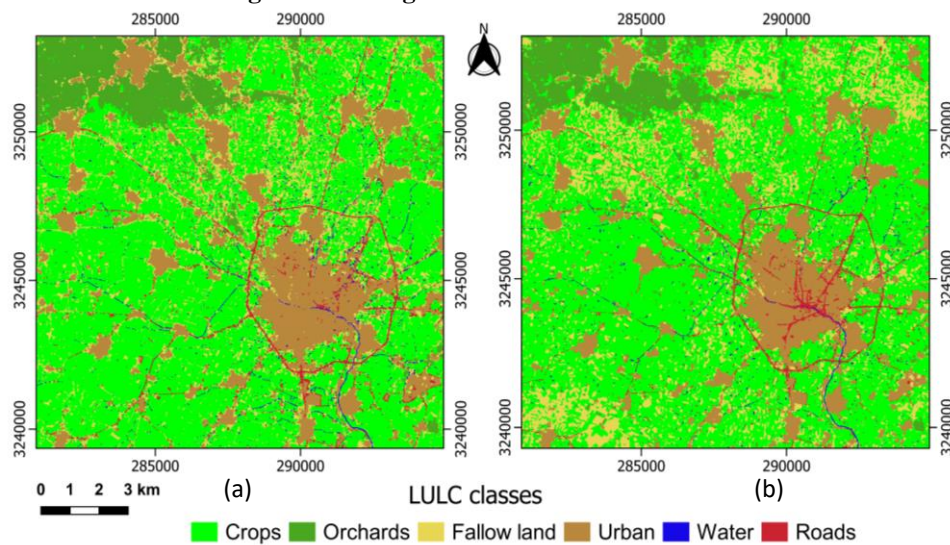

Figure 5. Land use/cover map of the study area using SVM and LMVM-b8 sharpened images acquired on (a) 03.02.2017 and (b) 12.08.2017

CONCLUSION

The current study investigated the potential of the sentinel-2 data for land use-cover classification under the conditions of arid regions and fragmented agricultural parcels. Different pan-sharpening techniques (Bayes, LMVM, RCS) were evaluated, in addition, various classification approaches (SVM, ANN, DT, RF) were applied and evaluated for land use/cover classification. The results showed that the Bayesian method produced higher spectral and spatial information in comparison to the original data. On the other hand, the results revealed high classification accuracy, as the SVM produced highest accuracy with overall accuracy of about 96% using LMVM-sharpened data. The applied methodology could be tested with extra datasets to find the proper fusion technique under similar conditions of the study area. Further investigation to utilize multi-temporal Sentinel-2 and Sentinel-1data in land use/cover mapping and agricultural crops monitoring is recommended.

REFERENCES

Chatziantoniou, A., Psomiadis, E. & Petropoulos, G. 2017. Co-orbital Sentinel 1 and 2 for LULC mapping with emphasis on wetlands in a Mediterranean setting based on machine learning. *Remote Sensing,* 9.

Chen, B., Huang, B. & XU, B. 2017. Multi-source remotely sensed data fusion for improving land cover classification. *ISPRS Journal of Photogrammetry and Remote Sensing,* 124**,** 27-39.

Chrysafis, I., Mallinis, G., Tsakiri, M. & Patias, P. 2019. Evaluation of single-date and multi-seasonal spatial and spectral information of Sentinel-2 imagery to assess growing stock volume of a Mediterranean forest. *International Journal of Applied Earth Observation and Geoinformation, 77*, 1-14.

Congedo, L. 2020. *Semi-Automatic Classification Plugin Documentation. DOI: http://dx.doi.org/ 10.13140/ RG.2.2.25480.65286/ 1* [Online]. [Accessed 08/08/ 2021].

Das, S. & Angadi, D. P. 2021. Land use land cover change detection and monitoring of urban growth using remote sensing and GIS techniques: a micro-level study. *Geojournal.*

Delincé, J. 2017. The cost-effectiveness of remote sensing in agricultural statistics. *In:* Delincé, J. (ed.) *Handbook on Remote Sensing for Agricultural Statistics.* Handbook of the Global Strategy to improve Agricultural and Rural Statistics (GSARS): Rome.

Demarez, V., Helen, F., Marais-Sicre, C. & Baup, F. 2019. In-Season mapping of irrigated crops using Landsat 8 and Sentinel-1 time series. *Remote Sensing,* 11.

Dibs, H., Hasab, H. A., Mahmoud, A. S. & Al-Ansari, N. 2021. Fusion methods and multi-classifiers to improve land cover estimation using remote sensing analysis. *Geotechnical and Geological Engineering.*

Duarte, L. & Teodoro, A. C. 2021. GIS open-source plugins development: A 10-year bibliometric analysis on scientific literature. *Geomatics,* 1, 206-245.

Duran, J., Buades, A., Coll, B., Sbert, C. & Blanchet, G. 2017. A survey of pansharpening methods with a new band-decoupled variational model. *Isprs Journal of Photogrammetry and Remote Sensing,* 125, 78-105.

Forkuor, G., Dimobe, K., Serme, I. & Tondoh, J. E. 2018. Landsat-8 vs. Sentinel-2: examining the added value of sentinel-2's red-edge bands to land-use and land-cover mapping in Burkina Faso. *Giscience & Remote Sensing,* 55, 331-354.

Gasparovic, M. & Jogun, T. 2018. The effect of fusing Sentinel-2 bands on land-cover classification. *International Journal of Remote Sensing,* 39, 822-841.

Gómez, C., White, J. C. & Wulder, M. A. 2016. Optical remotely sensed time series data for land cover classification: A review. *ISPRS Journal of Photogrammetry and Remote Sensing,* 116, 55-72.

Gumma, M. K., Tummala, K., Dixit, S., Collivignarelli, F., Holecz, F., Kolli, R. N. & Whitbread, A. M. 2020. Crop type identification and spatial mapping using Sentinel-2 satellite data with focus on field-level information. *Geocarto International.*

Jagalingam, P. & Hegde, A. V. 2015. A review of quality metrics for fused image. *International Conference on Water Resources, Coastal and Ocean Engineering (Icwrcoe'15),* 4, 133-142.

Karakus, P. & Karabork, H. 2016. Effect of pansharpened image on some of pixel based and object based classification accuracy. *ISPRS - International Archives of the Photogrammetry, Remote Sensing and Spatial Information Sciences,* XLI-B7, 235-239.

Lu, D. & Weng, Q. 2007. A survey of image classification methods and techniques for improving classification performance. *International Journal of Remote Sensing,* 28, 823-870.

Mazarire, T. T., Ratshiedana, P. E., Nyamugama, A., Adam, E. & Chirima, G. 2020. Exploring machine learning algorithms for mapping crop types in a heterogeneous agriculture landscape using Sentinel-2 data. A case study of Free State Province, South Africa. *South African Journal of Geomatics,* 9, 333-347.

Mercovich, R. A. 2015. Evaluation techniques and metrics for assessment of pan+MSI fusion (pansharpening). *Proc. SPIE 9472, Algorithms and Technologies for Multispectral, Hyperspectral, and Ultraspectral Imagery XXI, 94721I (21 May 2015); https://doi. org/10. 1117/12.2177093.*

Moumni, A. & Lahrouni, A. 2021. Machine learning-based classification for crop-type mapping using the fusion of high-resolution satellite imagery in a semiarid area. *Scientifica (Cairo),* 2021, 8810279.

Nguyen, H. V., Ulfarsson, M. O., Sveinsson, J. R. & Dalla Mura, M. 2021. Sentinel-2 sharpening using a single unsupervised convolutional neural network with MTF-based degradation model. *IEEE Journal of Selected Topics in Applied Earth Observations and Remote Sensing,* 14, 6882-6896.

Ni-Bin, C. & Kaixu, B. 2018. *Multisensor Data Fusion and Machine Learning for Environmental Remote Sensing,* CRC Press, CRC Press.

Nikolakopoulos, K. & Oikonomidis, D. 2017. Quality assessment of ten fusion techniques applied on Worldview-2. *European Journal of Remote Sensing,* 48, 141-167.

Noi, P. T. & Kappas, M. 2018. Comparison of random forest, k-nearest neighbor, and support vector machine classifiers for land cover classification using Sentinel-2 imagery. *Sensors,* 18.

Orynbaikyzy, A., Gessner, U., Mack, B. & Conrad, C. 2020. Crop type classification using fusion of Sentinel-1 and Sentinel-2 Data: assessing the impact of feature selection, optical data availability, and parcel sizes on the accuracies. *Remote Sensing,* 12.

Pan, L., Xia, H., Yang, J., Niu, W., Wang, R., Song, H., Guo, Y. & Qin, Y. 2021. Mapping cropping intensity in Huaihe basin using phenology algorithm, all Sentinel-2 and Landsat images in Google Earth Engine. *International Journal of Applied Earth Observation and Geoinformation,* 102.

Pohl, C. V. G., John, L. 2017. *Remote Sensing Image Fusion_ a Practical Guide,* CRC Press, CRC Press.

Rapinel, S. & Hubert-Moy, L. 2021. One-class classification of natural vegetation using remote sensing: a review. *Remote Sensing,* 13.

ROGAN, J. & CHEN, D. M. 2004. Remote sensing technology for mapping and monitoring land-cover and land-use change. *Progress in Planning,* 61, 301-325.

Steinhausen, M. J., Wagner, P. D., Narasimhan, B. & Waske, B. 2018. Combining Sentinel-1 and Sentinel-2 data for improved land use and land cover mapping of monsoon regions. *International Journal of Applied Earth Observation and Geoinformation,* 73, 595-604.

Sudhakar, S. & Kameshwara, R. S. 2010. Land use and land cover analysis. *In:* ROY, P. S., Dwivedi, R. S. & D.Vijayan (eds.) *Remote Sensing Applications.* NRSC/ISRO, Hyderabad, India.

Thakkar, A. K., Desai, V. R., Patel, A. & Potdar, M. B. 2017. Post-classification corrections in improving the classification of land use/land cover of arid region using RS and GIS: The case of Arjuni watershed, Gujarat, India. *The Egyptian Journal of Remote Sensing and Space Science,* 20**,** 79-89.

Vacca, A., Loddo, S., Melis, M. T., Funedda, A., Puddu, R., Verona, M., Fanni, S., Fantola, F., Madrau, S., Marrone, V. A., Serra, G., Tore, C., Manca, D., Pasci, S., Puddu, M. R. & Schirru, P. 2014. A GIS based method for soil mapping in Sardinia, Italy: a geomatic approach. *J Environ Manage,* 138**,** 87-96.

Valdivieso-Ros, C., Alonso-Sarria, F. & Gomariz-Castillo, F. 2021. Effect of different atmospheric correction algorithms on Sentinel-2 imagery classification accuracy in a semiarid Mediterranean area. *Remote Sensing,* 13.

Wan, H. M., Tang, Y. W., Jing, L. H., Li, H., Qiu, F. & Wu, W. J. 2021. Tree species classification of forest stands using multisource remote sensing data. *Remote Sensing,* 13.

Witharana, C., Civco, D. L. & Meyer, T. H. 2014. Evaluation of data fusion and image segmentation in earth observation based rapid mapping workflows. *ISPRS Journal of Photogrammetry and Remote Sensing,* 87**,** 1-18.

Worku, G., Bantider, A. & Temesgen, H. 2014. Effects of land use/land cover change on some soil physical and chemical properties in Ameleke micro-Watershed, Gedeo and Borena Zones, South Ethiopia. *Journal of Environment and Earth Science,* 4.

Wu, L., Yin, Y. Q., Jiang, X. Y. & Cheng, T. C. E. 2021. Pan-sharpening based on multi-objective decision for multi-band remote sensing images. *Pattern Recognition,* 118.

تعلم الآلة ودمج بيانات Sentinel-2 لإنتاج خرائط استخدام الأراضي في المناطق الجافة: دراسة حالة في الفيوم، مصر

علي جابر محمد محمود

قسم الأراضي والمياه ــ كلية الزراعة ــ جامعة الفيوم ــ الفيوم ــ مصر

تعد دراسة استخدامات الأراضي والغطاء الأرضي عنصرا أساسيا في مراقبة الموارد الطبيعية، وبالتالي وضع برامج الخدمة المناسبة لتلك الموارد. ولإنتاج مثل هذه الخرائط، فان الاستشعار عن بعد يساهم بشكل معنوي في الحصول على هذه المعلومات، إلا أن هناك بعض المحددات والاعتبارات التي يجب مراعاتها عند اختيار البيانات مثل تكلفة المرئيات الفضائية ودرجات الوضوح (مثل: المكانية والزمانية) لها، بالإضافة الي مدى توفر البرمجيات المطلوبة. وقد تم اختيار منطقة الدراسة في محافظة الفيوم، مصر، والتي تتميز بحيازات أراضي زراعية صغيرة، بالإضافة الي التغيرات السريعة في استخدامات الأراضي، خاصة خلال العشر سنوات الماضية. وفي الآونة الأخيرة، توفرت مرئيات Sentinel-2 ذات الدقة الطيفية العالية حيث تشتمل على 13 حزمة طيفية (band) بمستويات دقة 10، 20، 60 متر، مما يتيح ميزة لدراسة الحيازات الزراعية الصغيرة. وتهدف الدراسة الحالية الي استكشاف وتقييم مرئيات Sentinel-2 المجانية في دراسة استخدامات الأراضي باستخدام برنامج QGIS المجاني (مفتوح المصدر). في هذا الصدد، تم تقييم تقنيات دمج البيانات المختلفة (Bayes، LMVM، RCS) متبوعًا بتصنيف الصور باستخدام طرق مختلفة هي SVM وANN وDT وRF. وقد أظهرت النتائج أن طريقة Bayes وLMVM أنتجتا دقة طيفية ومكانية أعلى مقارنة بالبيانات الأصلية، على التوالي. بالإضافة إلى ذلك، أظهرت النتائج دقة تصنيف عالية، حيث أنتجت طريقة SVM أعلى دقة بلغت 96.8٪ باستخدام المرئيات المحسنة بطريقة LMVM. وبصفة عامة، يوصى بإجراء المزيد من الدراسات لاستخدام بيانات Sentinel-2 ذات تتابع زمني في رسم خرائط استخدام الأراضي الزراعية ومراقبتها.

الكلمات المفتاحية : Sentinel-2 ، QGIS ، الغطاء/الاستخدام الأرضي، الفيوم، مصر.